Acta Mech
https://doi.org/10.1007/s00707-019-02548-y

ORIGINAL PAPER

Junxiang Yang · Yibao Li · Chaeyoung Lee · Junseok Kim

Conservative Allen–Cahn equation with a nonstandard variable mobility

Received: 16 May 2019 / Revised: 30 August 2019

Abstract In this article, we present the conservative Allen–Cahn equation with a nonstandard variable mobility. Unlike the classical variable mobility, the proposed nonstandard variable mobility has a small value at the interface and a large value away from the interface. As benchmark tests, we perform temporal evolutions of two droplets without velocity field, 2D droplet deformation under a simple shear flow, 2D droplet deformation under a swirling flow, and 3D droplet deformation under a shear flow. The numerical results of the proposed method demonstrate a remarkable accuracy in preserving interfaces. Moreover, the proposed method not only captures interface location but also maintains uniform interface transition layer thickness.

1 Introduction

Multi-phase flow problems have wide applications in scientific research and industry. However, there are many difficulties in the simulation of multi-phase flow problems because of the complex interface dynamics. To numerically treat the morphological change of an interface, many numerical methods were developed: for example, the volume of fluid (VOF) method [1], the level set method (LSM) [2], the lattice Boltzmann method (LBM) [3], the immersed boundary method (IBM) [4], and the phase field method (PFM) [5]. The phase field (or diffuse interface) method has the merit of interface capturing. The topological change of the interface can be directly captured by solving the phase field equation without any artificial work. The two most famous models in the phase field method are the Cahn–Hilliard (CH) equation and the Allen–Cahn (AC) equation. In particular, the CH equation has been widely used to simulate multi-phase flow problems because of its property of mass conservation. Lee et al. [6] used the Cahn–Hilliard–Navier–Stokes (CHNS) model to numerically investigate the long-time dynamics of two-dimensional Rayleigh–Taylor instability. Alpak et al. [7] used the CHNS model to simulate the dynamics of two-phase flow in pore-scale media. Mu et al. [8] adopted the axisymmetric CHNS model to numerically study the effect of inflow velocity on the formation of a uniform droplet in a micro-device. In [9], the authors proposed a flux-corrected phase field method to improve the performance of phase field methods for simulating surface diffusion and they performed detailed numerical experiments. Because the classic AC equation cannot satisfy the mass conservation, its application in multi-phase fluid flow is severely limited. Recently, the authors in [10] have used the following modified AC equation with the Lagrange multiplier [11] for phase field modeling of two-phase flows and proposed a positivity-preserving conservative variational scheme:

J. Yang · C. Lee · J. Kim (✉)
Department of Mathematics, Korea University, Seoul 02841, Republic of Korea
E-mail: cfdkim@korea.ac.kr

Y. Li
School of Mathematics and Statistics, Xi'an Jiaotong University, Xi'an 710049, China

Published online: 18 November 2019

$$\frac{\partial \phi}{\partial t} = -\frac{F'(\phi)}{\epsilon^2} + \Delta\phi + \beta(t)\sqrt{F(\phi)}, \tag{1}$$

which is the well-known conservative AC (CAC) equation. Jeong and Kim [12] proposed a new CACNS model for two-phase flow. Aihara et al. [13] extended the CACNS model to simulate multi-component fluid flow. Although the binary conservative AC model satisfies mass conservation, it is limited to the simulation of a single droplet. Because the binary conservative AC model approximates the motion by mass conserving mean curvature flow, nonphysical growth and shrinking of droplets will occur when we use this model to simulate multiple droplets. To overcome the drawback of the binary conservative AC model, we propose a nonstandard mobility which minimizes the dynamics along the interface to preserve the interfacial profiles of multiple droplets.

In this paper, we present the CAC equation with nonstandard variable mobility:

$$\frac{\partial \phi}{\partial t} = M(\phi)\left[-\frac{F'(\phi)}{\epsilon^2} + \Delta\phi - |\nabla\phi|\nabla\cdot\left(\frac{\nabla\phi}{|\nabla\phi|}\right)\right] + \beta(t)\sqrt{F(\phi)}, \tag{2}$$

where $\phi(\mathbf{x}, t)$ is an order parameter which has the value 1 or -1 in the bulk phase and changes values from -1 to 1 in the diffusive region, $M(\phi)$ is a nonstandard mobility, $F(\phi) = 0.25(\phi^2 - 1)^2$ is a double well potential function, ϵ is a positive constant related to the thickness of diffusive interface, $\beta(t)$ is a non-constant Lagrange multiplier which enforces the mass conservation, and the anti-curvature term $|\nabla\phi|\nabla\cdot\left(\frac{\nabla\phi}{|\nabla\phi|}\right)$ is used to improve the capacity of the interface capturing. A standard variable mobility $M(\phi) = 1 - \phi^2$ was used in [14], and the dynamics is controlled by interfacial diffusion with this mobility. In this study, we use a nonstandard variable mobility $M(\phi) = \phi^2$, which is close to 1 in the bulk phase and decreases to 0 at the interface (see Fig. 1a). This new mobility is similar to the smoothed sign function $S(\psi^0) = \psi^0/\sqrt{(\psi^0)^2 + h^2}$ (see Fig. 1b) in the reinitialization equation for the level set method:

$$\frac{\partial \psi}{\partial \tau} = S(\psi^0)\left(1 - |\nabla\psi|\right), \tag{3}$$

where h is the space step size, τ is the fictitious time, and ψ^0 is the level set function before reinitialization. The smoothed sign function effectively keeps the interface location because $S(\psi^0)$ is close to zero at the interface. Please refer to [15] for more details about the reinitialization step in the level set method.

Furthermore, to improve the performance of the interface capturing, we include an anti-curvature term $|\nabla\phi|\nabla\cdot(\nabla\phi/|\nabla\phi|)$ in the following equation [16]:

$$\frac{\partial \phi}{\partial t} = -\frac{F'(\phi)}{\epsilon^2} + \Delta\phi - |\nabla\phi|\nabla\cdot\left(\frac{\nabla\phi}{|\nabla\phi|}\right). \tag{4}$$

The goal of this paper is to propose the CAC equation with a nonstandard variable mobility and an anti-curvature term so that we can not only maintain the interfaces but also keep interface location with well-defined interfacial transition layer. For comparison, we consider the following models: the models with

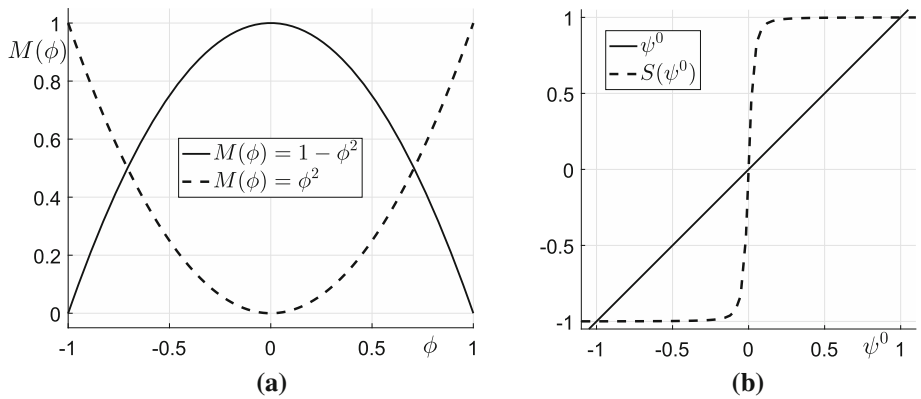

Fig. 1 **a** Standard $M(\phi) = 1 - \phi^2$ and nonstandard $M(\phi) = \phi^2$ variable mobilities, **b** smoothed sign function, $S(\psi^0)$

simple advection, with nonstandard mobility and without anti-curvature term, with constant mobility and anti-curvature term, and with standard mobility and anti-curvature term. Under the condition without velocity field, the evolution of two droplets is investigated to show that the proposed model can not only overcome the drawback of the CAC model but also maintain a good shape of interface. Under the condition with velocity field, the two-dimensional droplet deformation in simple shear flow and swirling flow and three-dimensional droplet deformation in shear flow are investigated to show that the proposed model can capture the interface, maintain the uniform interfacial transition layer, and preserve the mass.

The remaining parts of this paper are organized as follows: in Sect. 3, we give the numerical solution algorithm. To demonstrate the superior performance of the proposed model, we compare the numerical results in Sect. 4. In Sect. 5, conclusions are drawn.

2 Various mathematical models

In this section, we introduce various models which will be used in the following sections. First, we consider the following simple advection equation:

$$\frac{\partial \phi}{\partial t} + (u, v) \cdot \nabla \phi = 0, \tag{5}$$

where (u, v) is the velocity field. The discretization of Eq. (5) is described in Sect. 3. Second, we consider the following equation:

$$\frac{\partial \phi}{\partial t} + (u, v) \cdot \nabla \phi = -\frac{F'(\phi)}{\epsilon^2} + \Delta \phi - |\nabla \phi| \nabla \cdot \left(\frac{\nabla \phi}{|\nabla \phi|} \right) + \beta(t) \sqrt{F(\phi)}, \tag{6}$$

which implies $M(\phi) = 1$. Third, we consider the following equation:

$$\frac{\partial \phi}{\partial t} + (u, v) \cdot \nabla \phi = \phi^2 \left(-\frac{F'(\phi)}{\epsilon^2} + \Delta \phi \right) + \beta(t) \sqrt{F(\phi)}, \tag{7}$$

which implies $M(\phi) = \phi^2$ and there is no anti-curvature term $|\nabla \phi| \nabla \cdot (\nabla \phi / |\nabla \phi|)$. Fourth, we consider the equation with a standard mobility:

$$\frac{\partial \phi}{\partial t} + (u, v) \cdot \nabla \phi = (1 - \phi^2) \left[-\frac{F'(\phi)}{\epsilon^2} + \Delta \phi - |\nabla \phi| \nabla \cdot \left(\frac{\nabla \phi}{|\nabla \phi|} \right) \right] + \beta(t) \sqrt{F(\phi)}, \tag{8}$$

which implies $M(\phi) = 1 - \phi^2$. Finally, we consider the proposed equation:

$$\frac{\partial \phi}{\partial t} + (u, v) \cdot \nabla \phi = \phi^2 \left[-\frac{F'(\phi)}{\epsilon^2} + \Delta \phi - |\nabla \phi| \nabla \cdot \left(\frac{\nabla \phi}{|\nabla \phi|} \right) \right] + \beta(t) \sqrt{F(\phi)}, \tag{9}$$

which means $M(\phi) = \phi^2$.

3 Numerical solutions

In this section, we only introduce the numerical solution in two-dimensional space; the three-dimensional form is straightforward. Let $\Omega = (a, b) \times (c, d)$ be a computational domain, which is partitioned into a uniform mesh with a constant mesh spacing $h = (b - a)/N_x = (d - c)/N_y$, where N_x and N_y are the numbers of cells in x- and y-directions, respectively. For $i = 1, \ldots, N_x$ and $j = 1, \ldots, N_y$, let $(x_i, y_j) = (a + (i - 0.5)h, c + (j - 0.5)h)$ be the cell centers. Let ϕ_{ij}^n be an approximation of $\phi(x_i, y_j, n\Delta t)$, where $\Delta t = T/N_t$ is the temporal step size, T is the final time, and N_t is the total number of time steps. To solve Eq. (2), we use an operator splitting method, in which the original problem is split into a sequence of simpler problems [17]:

$$\frac{\partial \phi}{\partial t} = M(\phi) \left[-\frac{F'(\phi)}{\epsilon^2} + \Delta \phi - |\nabla \phi| \nabla \cdot \left(\frac{\nabla \phi}{|\nabla \phi|} \right) \right], \tag{10}$$

$$\frac{\partial \phi}{\partial t} = \beta(t)\sqrt{F(\phi)}. \tag{11}$$

First, we solve Eq. (10) by an explicit scheme:

$$\frac{\phi_{ij}^* - \phi_{ij}^n}{\Delta t} = M(\phi_{ij}^n)\left[-\frac{F'(\phi_{ij}^n)}{\epsilon^2} + \Delta_h \phi_{ij}^n - |\nabla_h \phi_{ij}^n| \nabla_h \cdot \left(\frac{\nabla_h \phi}{|\nabla_h \phi|}\right)_{ij}^n\right]. \tag{12}$$

The term $|\nabla_h \phi_{ij}^n| \nabla_h \cdot (\nabla_h \phi / |\nabla_h \phi|)_{ij}^n$ in Eq. (12) is calculated using the four vertex-centered gradients and is given by

$$|\nabla_h \phi_{ij}| = |\nabla_h \phi_{i+\frac{1}{2},j+\frac{1}{2}} + \nabla_h \phi_{i+\frac{1}{2},j-\frac{1}{2}} + \nabla_h \phi_{i-\frac{1}{2},j+\frac{1}{2}} + \nabla_h \phi_{i-\frac{1}{2},j-\frac{1}{2}}|/4$$

and

$$\begin{aligned}\nabla_h \cdot \left(\frac{\nabla_h \phi}{|\nabla_h \phi|}\right)_{ij} = \frac{1}{2h}\Bigg(&\frac{\phi^x_{i+\frac{1}{2},j+\frac{1}{2}} + \phi^y_{i+\frac{1}{2},j+\frac{1}{2}}}{\left|\nabla_h \phi_{i+\frac{1}{2},j+\frac{1}{2}}\right|} + \frac{\phi^x_{i+\frac{1}{2},j-\frac{1}{2}} - \phi^y_{i+\frac{1}{2},j-\frac{1}{2}}}{\left|\nabla_h \phi_{i+\frac{1}{2},j-\frac{1}{2}}\right|} \\ &- \frac{\phi^x_{i-\frac{1}{2},j+\frac{1}{2}} - \phi^y_{i-\frac{1}{2},j+\frac{1}{2}}}{\left|\nabla_h \phi_{i-\frac{1}{2},j+\frac{1}{2}}\right|} - \frac{\phi^x_{i-\frac{1}{2},j-\frac{1}{2}} + \phi^y_{i-\frac{1}{2},j-\frac{1}{2}}}{\left|\nabla_h \phi_{i-\frac{1}{2},j-\frac{1}{2}}\right|}\Bigg),\end{aligned}$$

where

$$\begin{aligned}\nabla_h \phi_{i+\frac{1}{2},j+\frac{1}{2}} &= \left(\phi^x_{i+\frac{1}{2},j+\frac{1}{2}}, \phi^y_{i+\frac{1}{2},j+\frac{1}{2}}\right) \\ &= \left(\frac{\phi_{i+1,j} + \phi_{i+1,j+1} - \phi_{ij} - \phi_{i,j+1}}{2h}, \frac{\phi_{i,j+1} + \phi_{i+1,j+1} - \phi_{ij} - \phi_{i+1,j}}{2h}\right).\end{aligned}$$

The other terms are similarly defined. Second, Eq. (11) is discretized as

$$\frac{\phi_{ij}^{n+1} - \phi_{ij}^*}{\Delta t} = \beta^* \sqrt{F(\phi_{ij}^*)}. \tag{13}$$

Using Eq. (13) and the mass conservation, we have

$$\sum_{i=1}^{N_x}\sum_{j=1}^{N_y} \phi_{ij}^0 = \sum_{i=1}^{N_x}\sum_{j=1}^{N_y} \phi_{ij}^{n+1} = \sum_{i=1}^{N_x}\sum_{j=1}^{N_y} \left(\phi_{ij}^* + \Delta t \beta^* \sqrt{F(\phi_{ij}^*)}\right). \tag{14}$$

Thus,

$$\beta^* = \frac{1}{\Delta t}\sum_{i=1}^{N_x}\sum_{j=1}^{N_y}(\phi_{ij}^0 - \phi_{ij}^*) \Big/ \sum_{i=1}^{N_x}\sum_{j=1}^{N_y} \sqrt{F(\phi_{ij}^*)}. \tag{15}$$

Finally, we get ϕ^{n+1} from Eq. (13), i.e., $\phi_{ij}^{n+1} = \phi_{ij}^* + \Delta t \beta^* \sqrt{F(\phi_{ij}^*)}$. Specifically, the discretization of the advection model in Sect. 2 is:

$$\frac{\phi_{ij}^{n+1} - \phi_{ij}^n}{\Delta t} + [(u, v) \cdot \nabla \phi]_{ij}^n = 0, \tag{16}$$

where $(u\phi_x + v\phi_y)_{ij}^n = u_{ij}^n \bar{\phi}_{x_{ij}}^n + v_{ij}^n \bar{\phi}_{y_{ij}}^n$, and the values $\bar{\phi}_{x_{ij}}^n$ and $\bar{\phi}_{y_{ij}}^n$ are computed using the upwind procedure, i.e.,

$$\bar{\phi}_{x_{ij}}^n = \begin{cases} (\phi_{ij}^n - \phi_{i-1,j}^n)/h & \text{if } u_{ij}^n > 0, \\ (\phi_{i+1,j}^n - \phi_{ij}^n)/h & \text{otherwise} \end{cases}$$

and

$$\bar{\phi}_{y_{ij}}^n = \begin{cases} (\phi_{ij}^n - \phi_{i,j-1}^n)/h & \text{if } v_{ij}^n > 0, \\ (\phi_{i,j+1}^n - \phi_{ij}^n)/h & \text{otherwise.} \end{cases}$$

4 Numerical experiment

In this section, we first perform the test of temporal evolutions of two droplets without velocity field; then, the droplet deformations in two-dimensional shear flow, swirling flow, and three-dimensional shear flow are conducted to verify the interface-preserving effect of the proposed method.

4.1 Temporal evolutions of two droplets without velocity field

In this test, the velocity field is absent. We consider the initial equilibrium state of two droplets with radii: 0.4 and 0.3. The initial condition is taken to be

$$\phi(x, y, 0) = \tanh\left(\frac{0.4 - \sqrt{(x+0.4)^2 + y^2}}{\sqrt{2}\epsilon}\right) + \tanh\left(\frac{0.3 - \sqrt{(x-0.6)^2 + y^2}}{\sqrt{2}\epsilon}\right) + 1 \tag{17}$$

on $\Omega = (-1, 1) \times (-1, 1)$. The parameters are $h = 1/64$, $\Delta t = 0.2h^2$, and $\epsilon = 0.0225$. The computations are performed until $t = 5000\Delta t$ for the following six cases: Case 1, $M(\phi) = 1$ without anti-curvature term; Case 2, $M(\phi) = 1$ with anti-curvature term; Case 3, $M(\phi) = 1 - \phi^2$ without anti-curvature term; Case 4, $M(\phi) = 1 - \phi^2$ with anti-curvature term; Case 5, $M(\phi) = \phi^2$ without anti-curvature term; and Case 6, $M(\phi) = \phi^2$ with anti-curvature term. Table 1 lists the details of the six cases above. Figures 2a–f show the evolutions of two droplets from Case 1 to Case 6, respectively. Figures 2g, h show the locally enlarged views of (e) and (f), respectively. In Figs. 2a, c, the anti-curvature term is absent and the equation changes into the CAC equation with a specific mobility; therefore, they approximate the motion by mass conserving curvature flow, i.e., the smaller droplet shrinks and the larger droplet grows with time. Because the effect of standard mobility $M(\phi) = 1 - \phi^2$ reduces the dynamics in bulk phase, we can observe that the evolution of two droplets in Figs. 2c is slower than that in Figs. 2a. Although the results in Figs. 2a, c obey the basic dynamics of the CAC equation, it does not satisfy the physical dynamics when we simulate some natural and engineering problems, such as bubble–liquid flow and droplets emulsion [18]. In Figs. 2b, d, the anti-curvature term is added to the equation to prevent the nonphysical evolution (i.e., smaller droplet shrinks and larger droplet grows); we can find that the interfaces of two droplets evolve away from the initial circular shapes. In Figs. 2e, f, the nonstandard mobility $M(\phi) = \phi^2$ is used. This approach lowers the dynamics along the interface; hence, we can find that the results in Figs. 2e, f are better than the other cases. Note that the result with the anti-curvature term is shown in Figs. 2f. The locally enlarged views in Figs. 2g, h show that our proposed model has the best interface-preserving effect.

In order to quantitatively show the temporal evolutions of the areas of two droplets, the polygonal area enclosed by the interface is defined as [4]:

$$A = \frac{1}{2}\left|\sum_{m}^{N}(X_m Y_{m+1} - Y_m X_{m+1})\right|, \tag{18}$$

where N is the total number of points on the interface; X and Y are the x- and y-coordinates, respectively. The temporal evolutions of the areas of two droplets for all cases are shown in Fig. 3. Because the anti-curvature term is absent and the standard mobility is used, the area of the smaller droplet decreases and the area of the larger droplet increases with time. When the anti-curvature term or the nonstandard mobility is used, the areas of the two droplets are almost preserved.

Table 1 Six cases for the evolutions of two droplets without velocity field

Case 1	$M(\phi) = 1$, without anti-curvature term
Case 2	$M(\phi) = 1$, with anti-curvature term
Case 3	$M(\phi) = 1 - \phi^2$, without anti-curvature term
Case 4	$M(\phi) = 1 - \phi^2$, with anti-curvature term
Case 5	$M(\phi) = \phi^2$, without anti-curvature term
Case 6	$M(\phi) = \phi^2$, with anti-curvature term

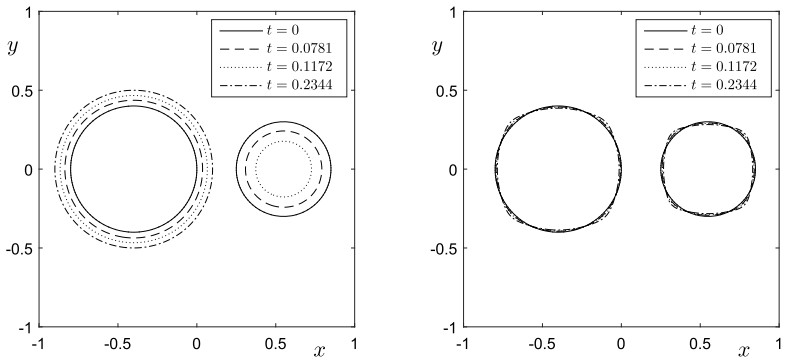

(a) $M(\phi) = 1$, no curvature term **(b)** $M(\phi) = 1$

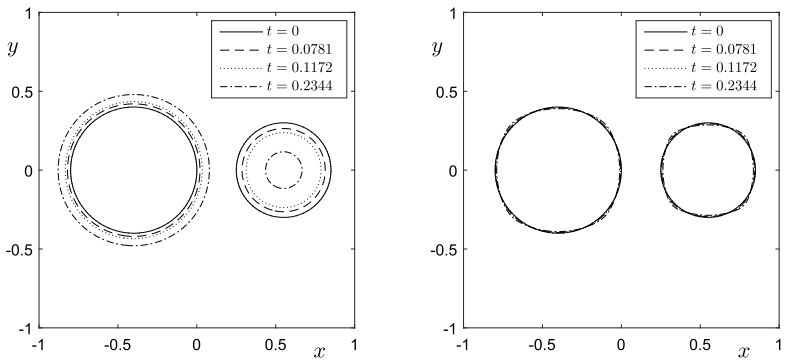

(c) $M(\phi) = 1 - \phi^2$, no curvature term **(d)** $M(\phi) = 1 - \phi^2$

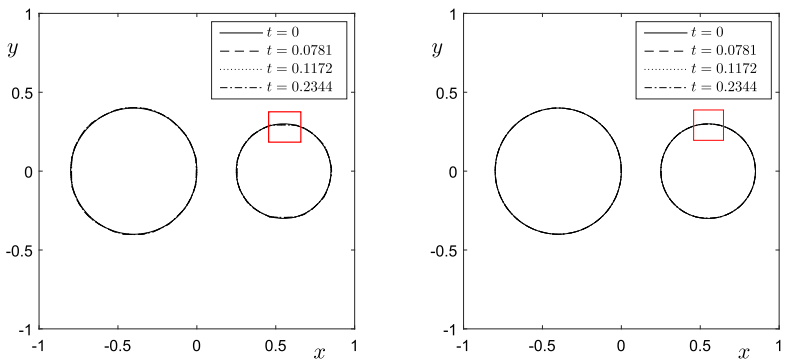

(e) $M(\phi) = \phi^2$, no curvature term **(f)** $M(\phi) = \phi^2$

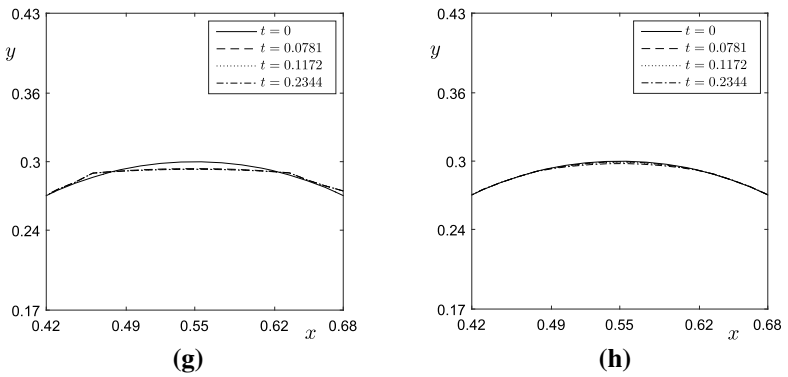

(g) **(h)**

Fig. 2 Temporal evolutions of two droplets without velocity field. Here, **g** and **h** are the locally enlarged views of the red box regions in **e** and **f**, respectively (color figure online)

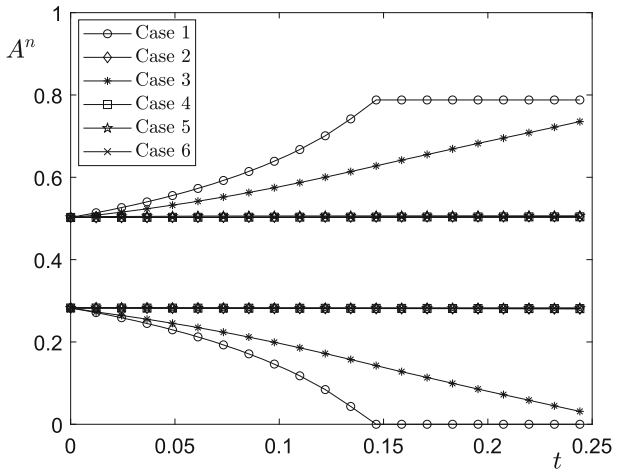

Fig. 3 Temporal evolutions of the areas of two droplets for all cases

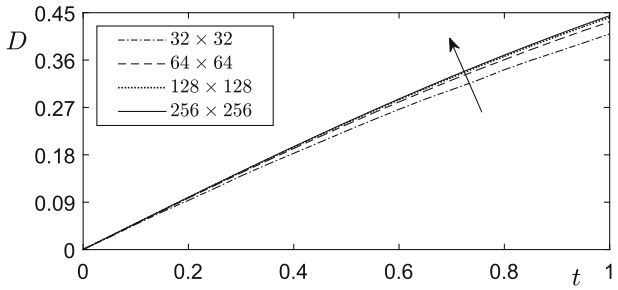

Fig. 4 Temporal evolutions of deformation parameter D with respect to different mesh sizes. The arrow indicates the direction of convergence

4.2 Convergence test

Now, we verify the proposed numerical method by performing a convergence test with respect to a series of finer mesh sizes: 32×32, 64×64, 128×128, and 256×256. We consider a droplet deformation under a background shear flow in the domain $\Omega = (-1, 1) \times (-1, 1)$ by using the model in Eq. (2). The deformation parameter is $D = (L - B)/(L + B)$, where L and B are the maximum and minimum droplet lengths, respectively. At the initial state, the droplet with a radius 0.5 is placed at the center of the domain. The velocity field is $(u(x, y, t),\ v(x, y, t)) = (y, 0)$. We use $\Delta t = 0.2h^2$ and $\epsilon = 0.075$. Figure 4 shows the temporal evolutions of deformation parameter D with respect to different mesh sizes. We can observe that the result is convergent with increasing in mesh size.

4.3 Two-dimensional droplet deformation in a simple shear flow

To demonstrate the performance of the proposed CAC equation with a nonstandard mobility for interface capturing in velocity field, we consider a droplet deformation under a background shear flow in two-dimensional space, i.e., $(u(x, y, t),\ v(x, y, t)) = (y, 0)$. The initial condition is a circular droplet on the computational domain $\Omega = (-2, 2) \times (-1, 1)$:

$$\phi(x, y, 0) = \tanh\left(\frac{0.5 - \sqrt{x^2 + y^2}}{\sqrt{2}\epsilon}\right). \tag{19}$$

For the top and bottom wall boundary conditions, we take the homogeneous Neumann boundary condition: $\phi_y(x, 1, t) = \phi_y(x, -1, t) = 0$. We impose the periodic boundary condition for the x-direction. Across the interfacial transition layer ϕ varies from -0.9 to 0.9 over a length of about $2\sqrt{2}\epsilon \tanh^{-1}(0.9)$. Therefore, if

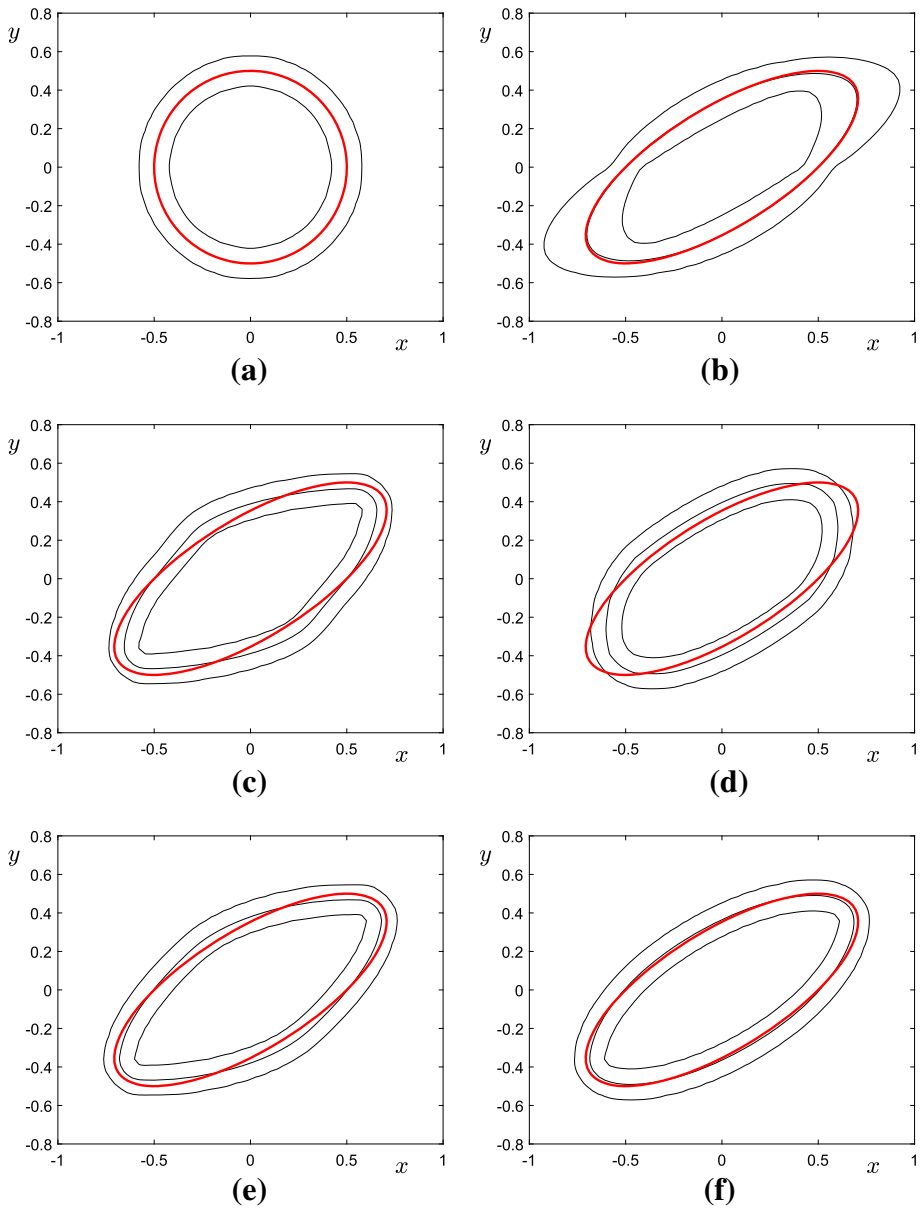

Fig. 5 **a** Initial condition, **b** simple advection, **c** $M(\phi) = 1$, **d** $M(\phi) = \phi^2$, no curvature term, **e** $M(\phi) = 1 - \phi^2$, **f** $M(\phi) = \phi^2$. Exact solution is represented by the red solid line (color figure online)

we want this value to be about hm, then $\epsilon = \epsilon_m = hm/[2\sqrt{2}\tanh^{-1}(0.9)]$ [12]. Figure 5a shows the contours at levels $\phi = -0.9,\ 0,\ 0.9$ of the initial profile. The parameter values used in this test are: $\epsilon = \epsilon_5$, $h = 1/32$, and $\Delta t = 0.2h^2$.

We now compare the numerical results from various models in Sect. 2. Note that the exact solution at $t = 1$ can be written as: $x = x_0 + ut = x_0 + y,\ y = y_0$, where x_0 and y_0 are the initial x- and y-coordinates of points on the interface. For the model of simple advection in Eq. (5), Fig. 5b shows the contours at $t = 1$ with the zero level contour of the exact solution. We can observe a good agreement with the exact solution. However, the contours at $\phi = -0.9$ and 0.9 are not good. The width of the contours is not uniform. The result of using the model Eq. (6) is not good as shown in Fig. 5c. The interface region has been too much relaxed. The model Eq. (7) results in shrinkage of interface due to the motion by mean curvature with mass conservation, please see Fig. 5d. The result using the model in Eq. (8) is shown in Fig. 5e, and we can observe that the result is not good. The interface region is still relaxed. Finally, for the proposed model Eq. (9), the result is good as

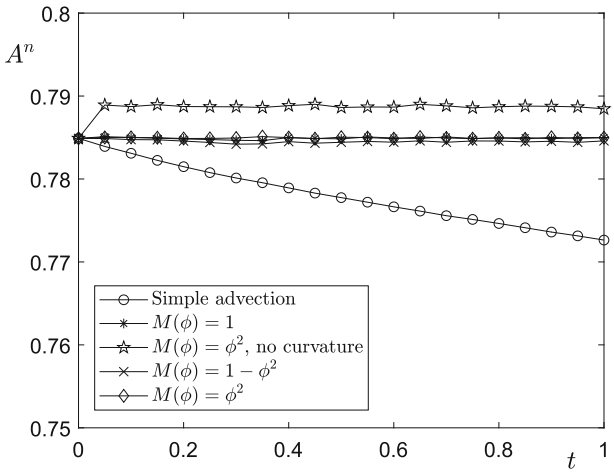

Fig. 6 Temporal evolutions of the area of droplet for different models

shown in Fig. 5f. The interface location is correctly moved, and the thickness of the interfacial transition layer is uniform.

The temporal evolutions of the area of droplet for different models are shown in Fig. 6. For the model of simple advection, the area decreases with time. For the model with nonstandard mobility $M(\phi) = \phi^2$ and without anti-curvature term, the area increases. For the other three models, the area is almost preserved with time. Comparing the results in Figs. 5 and 6, we can find that the proposed model has the merits of capturing the interface and preserving the area.

4.4 Two-dimensional droplet deformation in a swirling flow

Next, we consider the droplet deformation under a background swirling flow in the two-dimensional space $\Omega = (0, 1) \times (0, 1)$. The velocity field is defined as

$$u(x, y) = -2.5 \sin^2(\pi x) \sin(2\pi y), \quad v(x, y) = 2.5 \sin^2(\pi y) \sin(2\pi x). \tag{20}$$

We use the initial condition $\phi(x, y, 0) = \tanh((0.2 - \sqrt{(x - 0.5)^2 + (y - 0.7)^2})/(\sqrt{2}\epsilon))$ and parameters $h = 1/128$, $\Delta t = 0.2h^2$, $\epsilon = \epsilon_8$. The numerical tests are performed for Eqs. (5)–(9). The results at $t = 0.1709$ are shown in Fig. 7a–f. The exact solution is obtained by solving $dx/dt = u$ and $dy/dt = v$ using an improved Euler method with time step $\Delta t = 0.2h^2$. Comparing the numerical results obtained by Eqs. (5)–(8), we can observe that the result using Eq. (5) shows a good agreement with the exact solution; however, the transition layer thickness is not uniform. For the model Eqs. (6) and (8), although uniform transition layer thickness is achieved, the upper tip of droplet shrinks because of strong interfacial mobility. For the model Eq. (7), the result is not good because of the motion by mean curvature with mass conservation. However, the proposed model Eq. (9) not only maintains the uniform transition layer thickness, but also accurately captures the location of interface.

The temporal evolutions of the area of droplet for different models are shown in Fig. 8. For the model of simple advection, the area decreases with time. For the model with nonstandard mobility $M(\phi) = \phi^2$ and without anti-curvature term, the area increases. For the other three models, the area is almost preserved with time. Comparing the results in Figs. 7 and 8, we can find that the proposed model has the merits of capturing the interface and preserving the area.

4.5 Three-dimensional droplet deformation in a simple shear flow

Next, we further consider three-dimensional droplet deformation under a background shear flow. Here, we use $h = 1/32$, $\Delta t = 0.05h^2$, and $\epsilon = \epsilon_6$. The velocity field is defined on $\Omega = (0, 4) \times (0, 2) \times (0, 2)$:

$$u(x, y, z) = z - 1, \ v(x, y, z) = w(x, y, z) = 0, \tag{21}$$

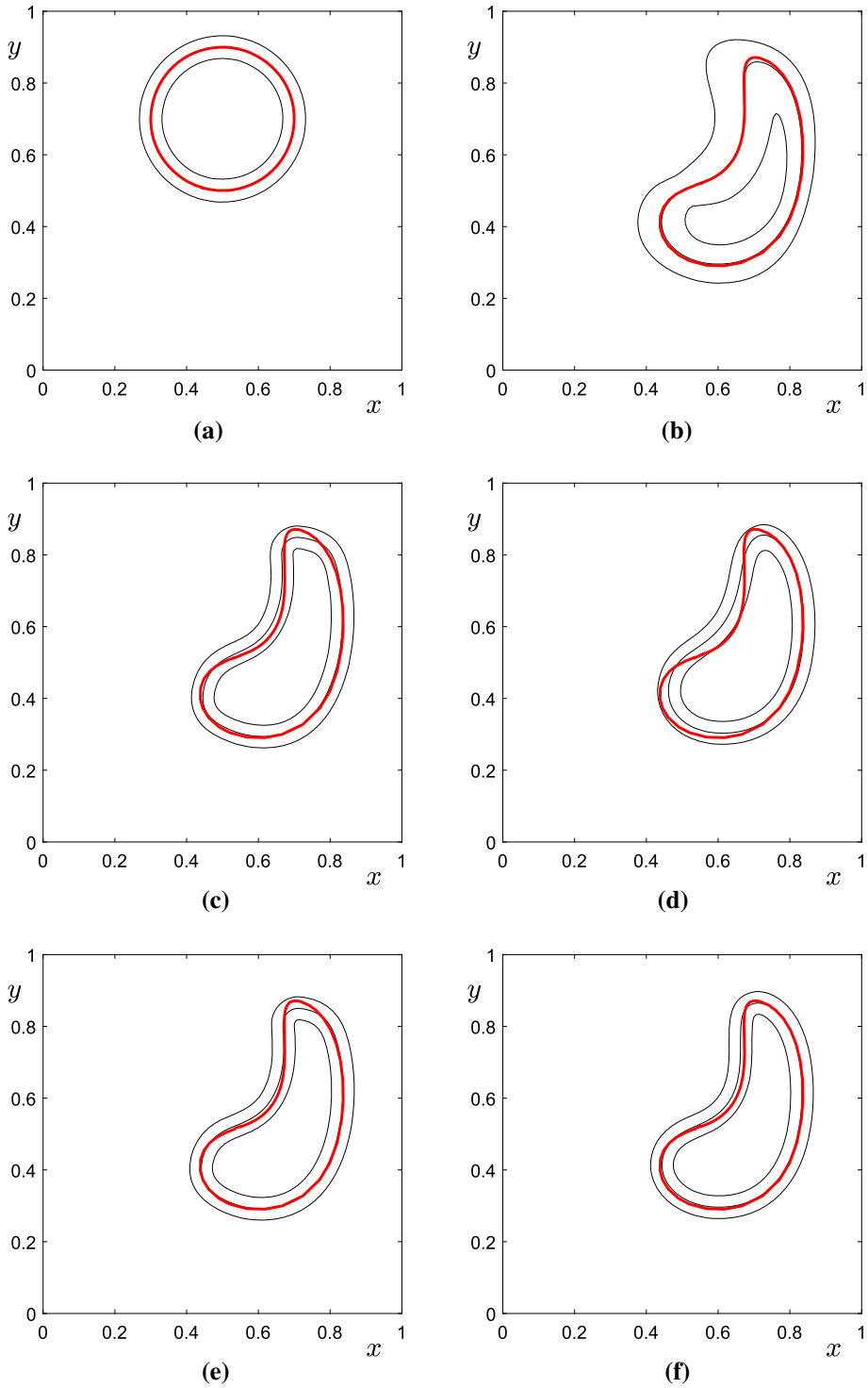

Fig. 7 **a** Initial condition, **b** simple advection, **c** $M(\phi) = 1$, **d** $M(\phi) = \phi^2$, no curvature term, **e** $M(\phi) = 1 - \phi^2$, **f** $M(\phi) = \phi^2$. Exact solution is represented by the red solid line (color figure online)

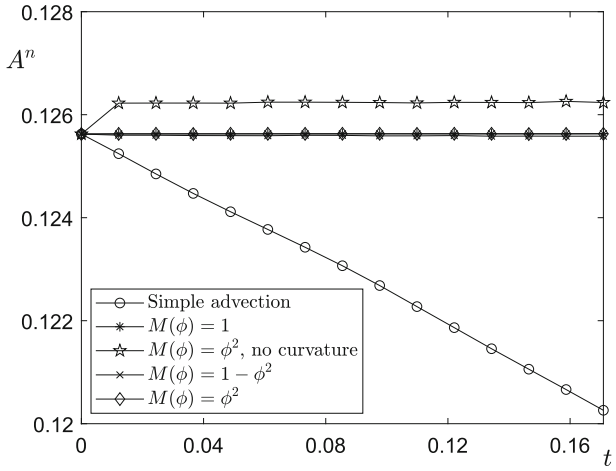

Fig. 8 Temporal evolutions of the area of droplet for different models

and the initial condition is chosen as

$$\phi(x, y, z, 0) = \tanh\left(\frac{0.5 - \sqrt{(x-2)^2 + (y-1)^2 + (z-1)^2}}{\sqrt{2}\epsilon}\right). \tag{22}$$

The numerical simulations for Eqs. (5)–(9) are performed until $t = 1$. The results are shown in Fig. 9, where the dark green, green, and yellow isosurfaces represent $\phi = 0.9, 0$, and -0.9 level sets, respectively. The slice profiles at $y = 1$ show the corresponding exact solution (the red solid line) and numerical solution (black solid line). As we can see, the proposed model (i.e., $M(\phi) = \phi^2$) shows the best agreement with the exact solution.

The temporal evolutions of the volume of droplet for different models are shown in Fig. 10. For the model of simple advection, the volume decreases with time. For the model with nonstandard mobility $M(\phi) = \phi^2$ and without anti-curvature term, the volume increases. For the other three models, the volume is almost preserved with time. Comparing the results in Figs. 9 and 10, we can find that the proposed model has the merits of capturing the interface and preserving the volume.

4.6 The deformation of four droplets in three-dimensional shear flow

In order to further verify the interface preserving and capturing of our model Eq. (9) in the velocity field, we investigate the deformation of four droplets in three-dimensional shear flow. The initial conditions on $\Omega = (0, 8) \times (0, 2) \times (0, 2)$ are set to be

$$\begin{aligned}\phi(x, y, z, 0) = &\tanh\left(\frac{0.5 - \sqrt{(x-1.3)^2 + (y-1)^2 + (z-1)^2}}{\sqrt{2}\epsilon}\right) \\ &+ \tanh\left(\frac{0.22 - \sqrt{(x-3.1)^2 + (y-1)^2 + (z-1.3)^2}}{\sqrt{2}\epsilon}\right) \\ &+ \tanh\left(\frac{0.4 - \sqrt{(x-4.7)^2 + (y-1)^2 + (z-0.8)^2}}{\sqrt{2}\epsilon}\right) \\ &+ \tanh\left(\frac{0.3 - \sqrt{(x-6.7)^2 + (y-1)^2 + (z-1.2)^2}}{\sqrt{2}\epsilon}\right) + 3,\end{aligned} \tag{23}$$

$$u(x, y, z) = y - 1, \ v(x, y, z) = w(x, y, z) = 0. \tag{24}$$

The computation is performed until $t = 0.4$ with the same parameters in Sect. 4.5. As shown in Fig. 11a, the droplets with different initial radii: $R = 0.5, 0.22, 0.4, 0.3$ are marked by a, b, c, d, respectively. Figure 11b shows the result at $t = 0.4$. Figure 11c shows the cross-sectional profile of (b) at $y = 1$. We can find that the

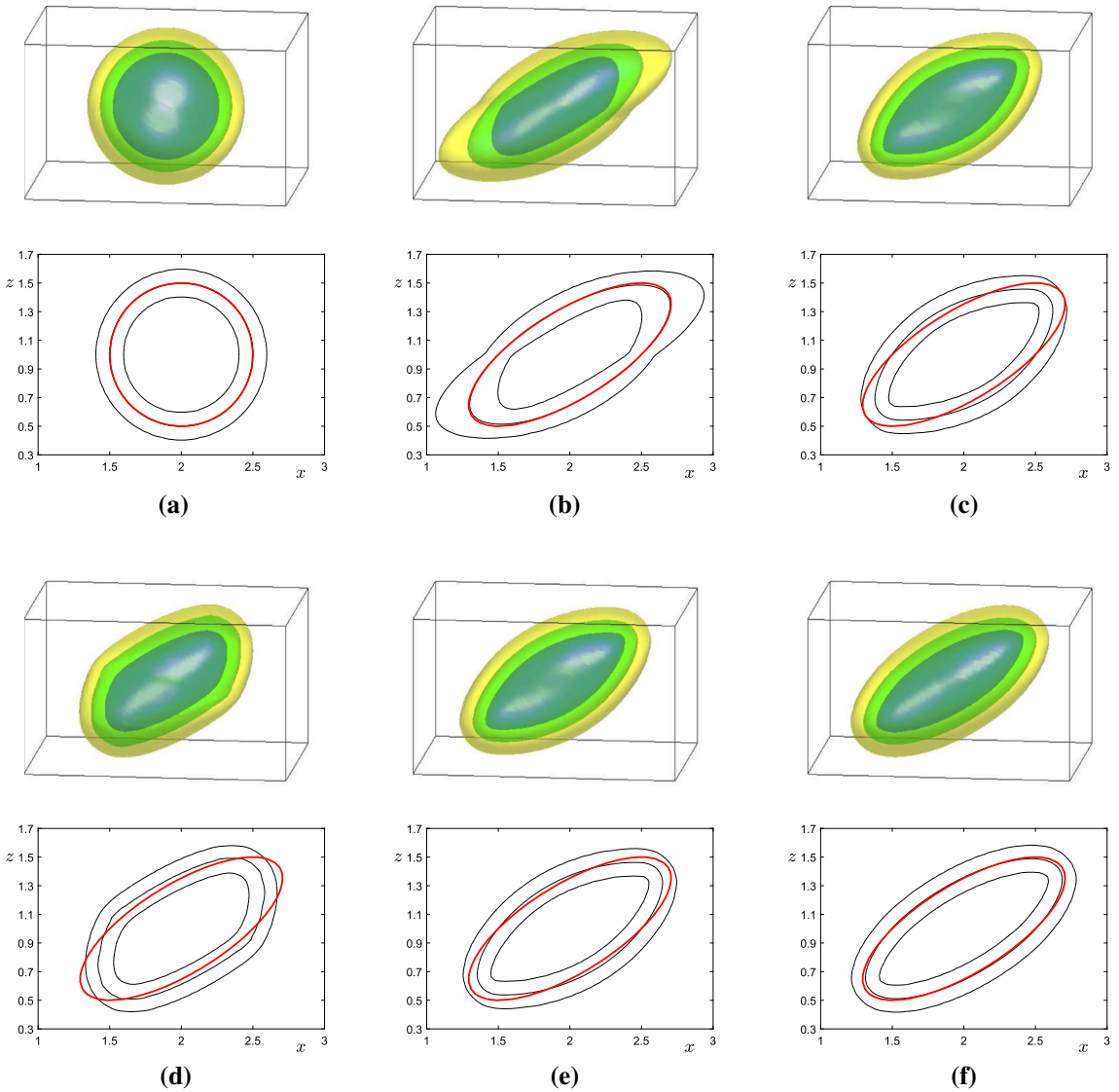

Fig. 9 **a** Initial condition, **b** simple advection, **c** $M(\phi) = 1$, **d** $M(\phi) = \phi^2$, no curvature term, **e** $M(\phi) = 1 - \phi^2$, **f** $M(\phi) = \phi^2$. Exact solution is represented by the red solid line. For interpretation of the references to color in this figure, the reader is referred to the Web version of this article

interface transition layer thickness is uniform and the interfacial positions show good agreement with exact solution. The temporal evolutions of volume V^n for each droplet are shown in Fig. 12; the result shows that the volumes enclosed by interface of each droplet are almost conserved.

4.7 Comparison with the conservative level set method

In order to verify the capacity of interface capturing of the proposed model, we consider the vortex droplet in a periodic swirling flow as in [2]. The initial conditions are set to be:

$$\phi(x, y, 0) = \tanh\left(\frac{0.15 - \sqrt{x^2 + (y - 0.25)^2}}{\sqrt{2}\epsilon}\right), \tag{25}$$

$$u(x, y, 0) = -\sin^2(\pi(x + 0.5))\sin(2\pi(y + 0.5)), \tag{26}$$

$$v(x, y, 0) = \sin^2(\pi(y + 0.5))\sin(2\pi(x + 0.5)) \tag{27}$$

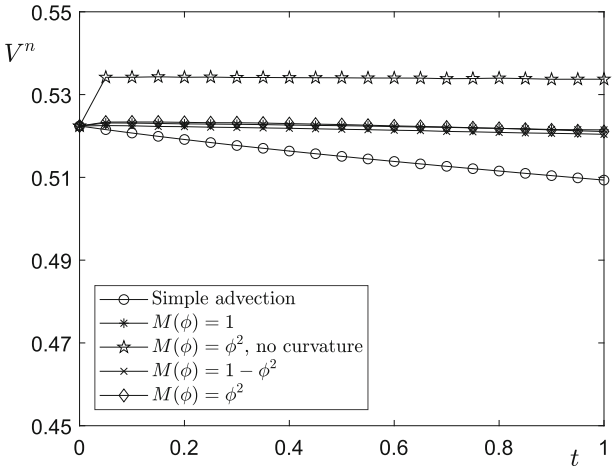

Fig. 10 Temporal evolutions of the volume of droplet for different models

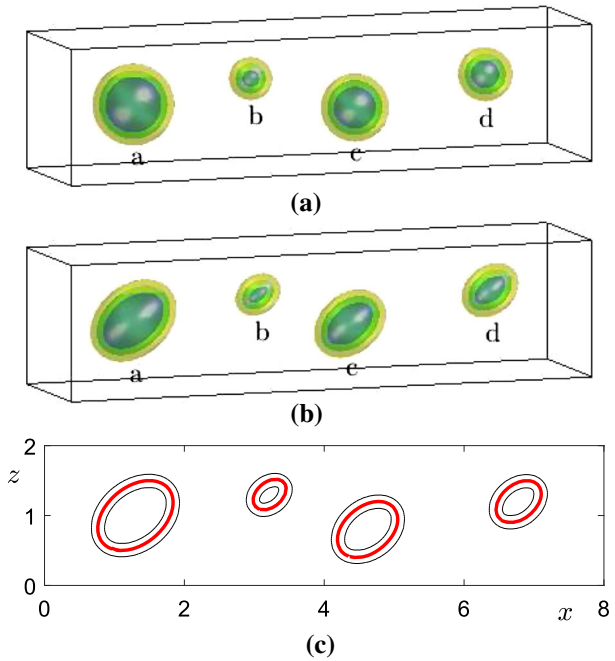

Fig. 11 Deformation of four droplets in three-dimensional shear flow. **a** Initial condition, **b** result at $t = 0.4$, **c** cross-profile. Exact solution is represented by the red solid line. For interpretation of the references to color in this figure, the reader is referred to the Web version of this article

on $\Omega = (-0.5, 0.5) \times (-0.5, 0.5)$. The velocity field will be reversed at $t = 2$. The parameters are $h = 1/128$, $\Delta t = 0.2h^2$, and $\epsilon = \epsilon_{10}$. The nonstandard mobility is scaled by $M(\phi) = \epsilon\phi^2/10$. Figure 13a shows the evolution of vortex droplet from the conservative level set method [2] where the mesh size 128×128 is used. The results from the proposed model are shown in Fig. 13b. We can observe that the proposed model has similar results with those from the conservative level set method [2].

4.8 Comparison with the previous result

Finally, we extend the proposed model to simulate the incompressible two-phase flow. After non-dimensionlization [6], the following system including the Navier–Stokes equation and the proposed model can be written as

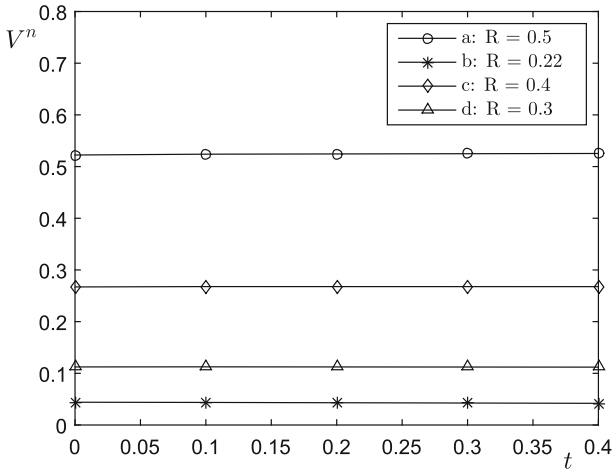

Fig. 12 Temporal evolutions of volume V^n for each droplet

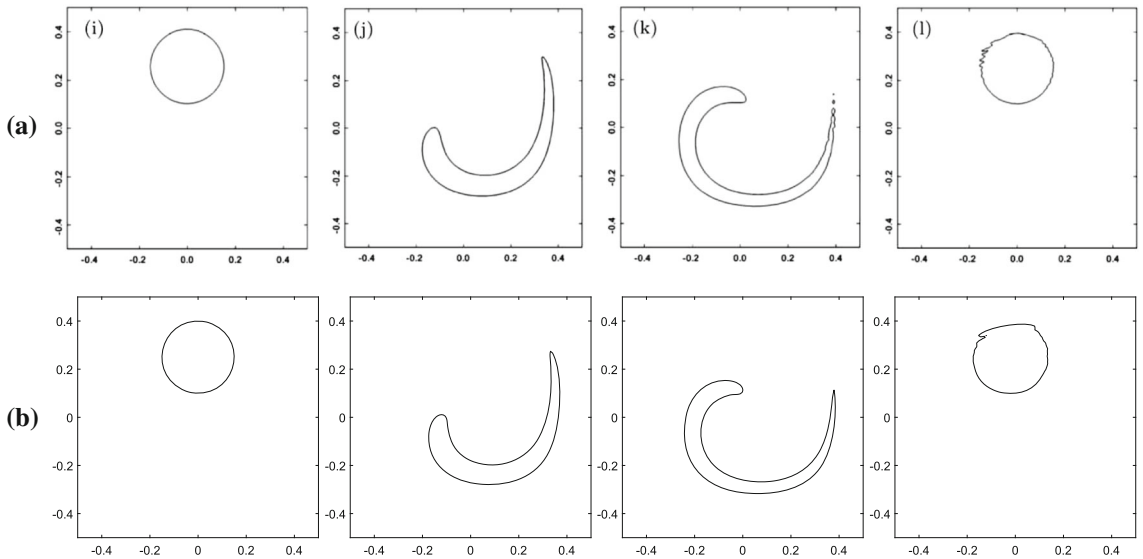

Fig. 13 Temporal evolutions of vortex droplet. **a** The results from the conservative level set method. Adapted from [2] with the permission of Elsevier Science, **b** the results from the proposed model

$$\nabla \cdot \mathbf{u} = 0, \tag{28}$$

$$\frac{\partial \mathbf{u}}{\partial t} = -\nabla p + \frac{1}{\mathrm{Re}}\Delta \mathbf{u} + \mathbf{SF}(\phi) - \mathbf{u} \cdot \nabla \mathbf{u}, \tag{29}$$

$$\frac{\partial \phi}{\partial t} = \frac{\phi^2}{\mathrm{Pe}}\left[-\frac{F'(\phi)}{\epsilon^2} + \Delta\phi - |\nabla\phi|\nabla \cdot \left(\frac{\nabla\phi}{|\nabla\phi|}\right)\right] + \beta(t)\sqrt{F(\phi)}, \tag{30}$$

where $\mathbf{u}$ is the velocity, p is the pressure, Re is the Reynolds number, Pe is the Peclet number. The surface tension term is defined as [19]

$$\mathbf{SF}(\phi) = -\frac{3\sqrt{2}\epsilon}{4\mathrm{We}}\nabla \cdot \left(\frac{\nabla\phi}{|\nabla\phi|}\right)|\nabla\phi|\nabla\phi, \tag{31}$$

where We is the Weber number. For the numerical solution of the Navier–Stokes equation, please see [6]. Now, we consider a benchmark problem of the droplet deformation in a shear flow from Sheth and Pozrikidis [20]. The initial conditions are

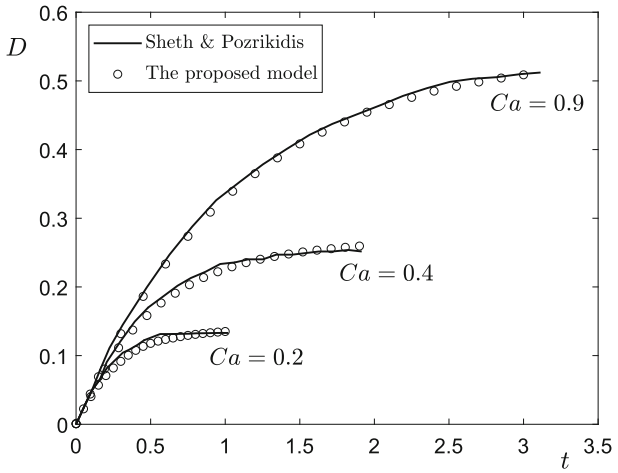

Fig. 14 Temporal evolutions of the droplet deformation for Re = 1, Ca = 0.2, 0.4, and 0.9

$$\phi(x, y, 0) = \tanh\left(\frac{0.5 - \sqrt{x^2 + y^2}}{\sqrt{2}\epsilon}\right), \tag{32}$$

$$u(x, y, 0) = y, \quad v(x, y, 0) = 0 \tag{33}$$

on the domain $\Omega = (-2, 2) \times (-1, 1)$. The parameters are: $h = 1/32$, $\Delta t = 0.2h^2$, Re = 1, and $\epsilon = \epsilon_4$. For three different Capillary numbers Ca = We/Re = 0.2, 0.4, 0.9, the Peclet numbers Pe = 6.8, 30, and 100 are used, respectively. In Fig. 14, the solid lines are the temporal evolutions of the deformation parameter from Sheth and Pozrikidis [20]. The open circles are our results. As we can see, they are in good agreement.

5 Conclusions

In this paper, we considered the CAC equation with a nonstandard variable mobility. Unlike the classical variable mobility, the proposed nonstandard variable mobility has small value at the interface and large value away from the interface. As benchmark tests, we performed temporal evolutions of two droplets without velocity field, 2D droplet deformation under a simple shear flow, 2D droplet deformation under a swirling flow, and 3D droplet deformation under a shear flow. The numerical results of the proposed method demonstrated remarkable accuracy in preserving the interfaces. Moreover, the proposed method not only accurately captures interface location but also maintains uniform interface transition layer thickness. As future research directions, the proposed model can be used in modeling and simulation of two-phase fluid flows [21–25].

Acknowledgements Y. B. Li is supported by National Natural Science Foundation of China (Nos. 11601416, 11631012). The corresponding author (J. S. Kim) was supported by Basic Science Research Program through the National Research Foundation of Korea (NRF) funded by the Ministry of Education (NRF-2019R1A2C1003053).

References

1. Pathak, A., Raessi, M.: A 3D, fully Eulerian, VOF-based solver to study the interaction between two fluids and moving rigid bodies using the fictitious domain method. J. Comput. Phys. **311**, 87–113 (2016)
2. Tabar, N.S., Vasilyev, O.V.: Stabilized conservative level set method. J. Comput. Phys. **375**, 1033–1044 (2018)
3. Chen, Z., Shu, C., Tan, D., Niu, X.D., Li, Q.Z.: Simplified multiphase lattice Boltzmann method for simulating multiphase flows with large density ratios and complex interfaces. Phys. Rev. E **98**, 063314 (2018)
4. Li, Y., Jung, E., Lee, W., Lee, H.G., Kim, J.: Volume preserving immersed boundary methods for two-phase fluid flows. Int. J. Numer. Methods Fluids **69**, 842–858 (2012)
5. Kim, J.: Phase-field models for multi-component fluid flows. Commun. Comput. Phys. **12**, 613–661 (2012)
6. Lee, H.G., Kim, J.: On the long time simulation of Rayleigh–Taylor instability. Int. J. Numer. Methods Eng. **85**, 1633–1647 (2011)
7. Alpak, F.O., Riviere, B., Frank, F.: A phase-field method for the direct simulation of two-phase flows in pore-scale media using a non-equilibrium wetting boundary condition. Comput. Geosci. **20**, 881–908 (2016)

8. Mu, K., Si, T., Li, E., Xu, R.X., Ding, H.: Numerical study on droplet generation in axisymmetric flow focusing upon actuation. Phys. Fluids **30**, 012111 (2018)
9. Zhang, Y., Ye, W.: A flux-corrected phase-field method for surface diffusion. Commun. Comput. Phys. **22**, 422–440 (2017)
10. Joshi, V., Jaiman, R.K.: A positivity preserving and conservative variational scheme for phase-field modeling of two-phase flows. J. Comput. Phys. **360**, 137–166 (2018)
11. Brassel, M., Bretin, E.: A modified phase field approximation for mean curvature flow with conservation of the volume. Math. Mehtods Appl. Sci. **34**, 1157–1180 (2011)
12. Jeong, D., Kim, J.S.: Conservative Allen–Cahn–Navier–Stokes system for incompressible two-phase fluid flows. Comput. Fluids **156**, 239–246 (2017)
13. Aihara, S., Takaki, T., Takada, N.: Multi-phase-field modeling using a conservative Allen–Cahn equation for multiphase flow. Comput. Fluids **178**, 141–151 (2019)
14. Ceniceros, H., Garíca-Cervera, C.: A new approach for the numerical solution of diffusion equations with variable and degenerate mobility. J. Comput. Phys. **246**, 1–10 (2013)
15. Tsui, Y.Y., Liu, C.Y., Lin, S.W.: Coupled level-set and volume-of-fluid method for two-phase flow calculations. Numer. Heat Transf. B **71**, 173–185 (2017)
16. Chiu, P.H., Lin, Y.T.: A conservative phase field method for solving incompressible two-phase flows. J. Comput. Phys. **230**, 185–204 (2011)
17. Kim, J.S., Lee, S., Choi, Y.: A conservative Allen–Cahn equation with a space–time dependent Lagrange multiplier. Int. J. Eng. Sci. **84**, 11–17 (2014)
18. Rosti, M.E., Vita, F.D., Brandt, L.: Numerical simulations of emulsions in shear flows. Acta Mech. **230**, 667–682 (2019)
19. Kim, J.: A continuous surface tension force formulation for diffuse-interface model. J. Comput. Phys. **204**, 784–804 (2005)
20. Sheth, K.S., Pozrikidis, C.: Effects of inertia on the deformation of liquid drops in simple shear flow. Comput. Fluids **24**(2), 101–19 (1995)
21. Deng, Y., Liu, Z., Wu, Y.: Topology optimization of capillary, two-phase flow problems. Commun. Comput. Phys. **22**, 1413–1438 (2017)
22. Geier, M., Fakhari, A., Lee, T.: Conservative phase-field lattice Boltzmann model for interface tracking equation. Phys. Rev. E **91**, 063309 (2015)
23. Morvant, A., Seal, E., Walker, S.W.: A coupled Ericksen/Allen–Cahn model for liquid crystal droplets. Appl. Math. Appl. **75**, 4048–4065 (2018)
24. Vasconcelos, D.F.M., Rossa, A.L., Coutinho, A.L.G.A.: A residual-based Allen–Cahn phase field model for the mixture of incompressible fluid flows. Int. J. Numer. Methods Fluids **75**, 645–667 (2014)
25. Soligo, G., Roccon, A., Soldati, A.: Mass-conservation-improved phase field methods for turbulent multiphase flow simulation. Acta Mech. **230**, 683–696 (2019)